ELSEVIER

Chemical Engineering Journal 79 (2000) 133–143

Chemical Engineering Journal

www.elsevier.com/locate/cej

Characterization of dynamic gas–solid distribution in fluidized beds

Heping Cui, Navid Mostoufi, Jamal Chaouki*

Department of Chemical Engineering, Biopro Research Center, Ecole Polytechnique de Montreal, CP 6079, succ. Centre-ville, Montreal, Que., Canada H3C 3A7

Received 25 November 1999; received in revised form 23 March 2000; accepted 31 March 2000

Abstract

A probability distribution model of the local voidage was proposed to describe and simulate dynamic gas–solid distribution in the bubbling and turbulent fluidized bed reactors. Experiments were carried out in an air-fluidized bed. The bed materials were FCC particles (Geldart A) and irregular sand particles (Geldart B). A cross-optical fiber probe was employed to measure dynamic voidage. The minimum probability method was introduced to identify the division between the emulsion phase and the bubble phase. The statistical analysis indicated that the two particle types employed have extremely different dynamic behaviors corresponding to different gas–solid distributions and the interaction between the bubble and emulsion phases. For the FCC particles, the voidage of the emulsion phase is very close to that at the minimum fluidization with little effect from the formation and motion of bubbles in bubbling regime, and deviates a little from ε_{mf} in turbulent regime. For the sand particles, the voidage of the emulsion phase differs far from that at the minimum fluidization, and the bubble phase gradually becomes more dilute from bubbling to turbulent regime. However, for both particles the dynamic voidage fluctuations in the emulsion phase and the bubble phase followed beta distribution under various operating conditions. The probability density functions of the local voidage from ε_{mf} to 1 showed the continuous double-peak phenomena, one peak for the emulsion phase and another for the bubble phase, and evolved with changing operating conditions and bed position. A particular distribution, called coupled beta distribution, was developed to describe and simulate such probability density function with double peaks and its complex evolution from bubbling to turbulent regime. The quantification of the probability density function then statistically introduced the spatiotemporal two-phase flow structure.

Keywords: Fluidization; Gas–solid distribution; Probability distribution model; Coupled beta distribution; Dynamic two-phase structure

1. Introduction

Gas–solid fluidized bed reactors have found a wide range of industrial applications. However, the heat/mass transfer and reaction within such reactors are far from being well understood and effectively quantified due to the complexity of the gas–solid interactions. Many models with simple assumptions have been suggested to describe the behavior of the two phases. These models have been widely introduced in the literature [1–4]. They have explained and made sense of the main features of the bubble and emulsion phases in fluidized beds and have been of great help in improving knowledge of the interaction between the two phases.

The traditional two-phase theory assumes the existence of only two phases in the fluidized bed, i.e., solid-free bubbles ($\varepsilon=1$) and emulsion phase at minimum fluidization ($\varepsilon=\varepsilon_{mf}$). However, this assumption is an oversimplification of what actually happens in the bed. In fact, the existence of solid particles in the bubbles has been shown both experimentally [5–7] and theoretically [8,9]. The emulsion also does not stay at minimum fluidization state, but can contain more gas at higher gas velocities [10,11]. This phenomena results in a dynamic distribution of the two phases with the voidage. The dynamic gas–solid distribution can have a considerable effect on the apparent reaction and heat/mass transfer rate in the fluidized beds. The traditional two-phase theory is incapable of predicting these rates properly. Another shortcoming of the simplified two-phase theory is that it is mostly limited to explain the low-velocity bubbling fluidization and is not able to explain the evolution of the two phases upon increasing the gas velocity. Increasing the superficial gas velocity in a fluidized bed causes a better mixing of the two phases which results in more solid particles entering the bubbles and more gas entering the emulsion phase. As a result, a wider dynamic distribution can be observed by increasing the gas velocity, while the simple two-phase model is unable to justify it.

* Corresponding author. Tel.: +1-514-340-4711, ext: 4034; fax: +1-514-340-4159.
E-mail address: chaouki@biopro.polymtl.ca (J. Chaouki)

1385-8947/00/$ – see front matter
PII: S1385-8947(00)00178-9

In the recent years, more works have focused on the dynamic behavior of the two-phase flow structures in actual fluidized processes in order to improve the understanding of the interaction between the two phases [12–15]. Some of these studies have demonstrated the complexity of the gas–solid distribution in the gas–solid fluidized beds [11,16,17]. A better understanding of how solids disperse in the bubbles and how gas enters the emulsion has an enormous impact on the practical use of the fluidized bed reactors [4], which is also highly valuable for improving the traditional two-phase model for industrial applications. Therefore, this paper focuses on quantitative description of the dynamic gas–solid distribution of the two phases in the bubbling and turbulent fluidization regimes by analyzing the probability distribution function of the local voidage from ε_{mf} to 1.

2. Probability distribution model

The simple two-phase model assumes the existence of two extreme phases, namely the solid-free bubble phase (ε=1) and the emulsion phase at minimum fluidization (ε=ε_{mf}). Throughout this paper, we refer to the solid-free bubbles as *pure bubble* phase and the emulsion at minimum fluidization as *saturated emulsion*. Of course, one has to remember that a bubble consists of a core gas region surrounded by the cloud, in which the particles exist. The particles can penetrate into different bubble regions. However, in the middle of the bubble there may be a gas core in which no particle enters. Evidence will be given later in Section 4 for the existence of such gas core. Therefore, the phrase "pure bubble" in this paper refers to that portion of the bubble that "contains absolutely no solids" and should not be confused with the whole bubble as if it does not contain any particle.

In the simplified two-phase theory, the distribution of the voidage in the fluidized bed is assumed to be equal to either 1 or ε_{mf}, as illustrated by the dashed line in Fig. 1. The corresponding cumulative probability distribution function could be expressed by a simplified two-phase model as follows:

$$\mathrm{Pr}^0(\varepsilon) = \mathrm{Pr_e}^0(\varepsilon) + \mathrm{Pr_b}^0(\varepsilon) \tag{1}$$

in which

$$\mathrm{Pr_e}^0(\varepsilon) = f^0 \tag{2}$$

$$\mathrm{Pr_b}^0(\varepsilon) = \begin{cases} 0, & \varepsilon_{mf} \le \varepsilon < 1 \\ 1 - f^0, & \varepsilon = 1 \end{cases} \tag{3}$$

where $\mathrm{Pr}^0(\varepsilon)$, $\mathrm{Pr_e}^0(\varepsilon)$, and $\mathrm{Pr_b}^0(\varepsilon)$ are the cumulative probability distribution functions of the local voidage for the overall, saturated emulsion phase, and pure bubble phase, respectively, and f^0 is the emulsion phase fraction:

$$f^0 = \frac{1 - \varepsilon_r}{1 - \varepsilon_{mf}} \tag{4}$$

where ε_r is the time-averaged voidage at an arbitrary local position.

The actual flow structure in fluidized beds show highly complicated spatiotemporal dynamic behavior due to the nonlinearity of the gas–solid interaction. The emulsion and bubble phases, with various irregular structures at different time and position, exhibit not only extreme behavior with the voidages ε_{mf} or 1, but also dynamic behavior with a series of voidages in between [18], corresponding to dynamic gas–solid distribution, as shown in Fig. 1. Therefore, we introduced a probability distribution model of the local voidage varying from ε_{mf} to 1 in order to describe the cumulative probability distributions of the complex gas–solid distribution of the two-phase flow structure as the following:

$$\mathrm{Pr}(\varepsilon)\frac{1}{1 - \varepsilon_{mf}}\int_{\varepsilon_{mf}}^{\varepsilon} \mathrm{pr}(\varepsilon)\,\mathrm{d}\varepsilon \tag{5}$$

Eq. (5) can also be expressed as

$$\mathrm{Pr}(\varepsilon) = \mathrm{Pr_e}(\varepsilon) + \mathrm{Pr_b}(\varepsilon) \tag{6}$$

where

$$\mathrm{Pr_e}(\varepsilon) = \frac{f}{1 - \varepsilon_{mf}}\int_{\varepsilon_{mf}}^{\varepsilon} \mathrm{pr_e}(\varepsilon)\,\mathrm{d}\varepsilon \tag{7}$$

$$\mathrm{Pr_b}(\varepsilon) = \frac{1 - f}{1 - \varepsilon_{mf}}\int_{\varepsilon_{mf}}^{\varepsilon} \mathrm{pr_b}(\varepsilon)\,\mathrm{d}\varepsilon \tag{8}$$

thus

$$\begin{aligned}\mathrm{Pr}(\varepsilon) &= \frac{f}{1 - \varepsilon_{mf}}\int_{\varepsilon_{mf}}^{\varepsilon} \mathrm{pr_e}(\varepsilon)\,\mathrm{d}\varepsilon + \frac{1 - f}{1 - \varepsilon_{mf}}\int_{\varepsilon_{mf}}^{\varepsilon} \mathrm{pr_b}(\varepsilon)\,\mathrm{d}\varepsilon \\ &= \frac{1}{1 - \varepsilon_{mf}}\int_{\varepsilon_{mf}}^{\varepsilon} (f\,\mathrm{pr_e}(\varepsilon) + (1 - f)\mathrm{pr_b}(\varepsilon))\,\mathrm{d}\varepsilon \end{aligned} \tag{9}$$

$$\mathrm{pr}(\varepsilon) = f\,\mathrm{pr_e}(\varepsilon) + (1 - f)\mathrm{pr_b}(\varepsilon) \tag{10}$$

where $\mathrm{Pr}(\varepsilon)$, $\mathrm{Pr_e}(\varepsilon)$, and $\mathrm{Pr_b}(\varepsilon)$ are the cumulative probability distribution functions of the local voidage of the overall, the emulsion phase and the bubble phase, respectively, while $\mathrm{pr}(\varepsilon)$, $\mathrm{pr_e}(\varepsilon)$, and $\mathrm{pr_b}(\varepsilon)$ are the corresponding probability

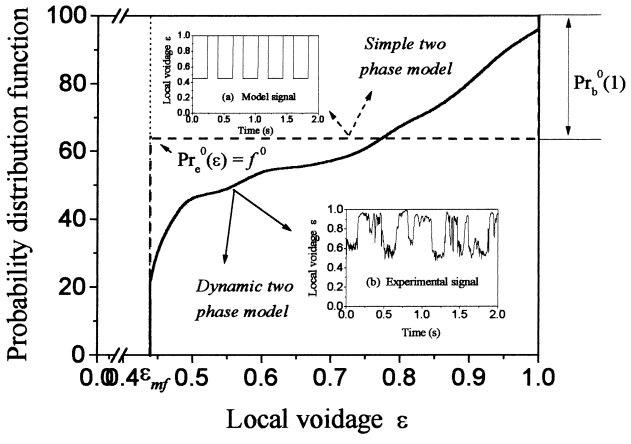

Fig. 1. Probability distribution model of the local voidage ε.

density functions, $\varepsilon_{mf} \leq \varepsilon \leq 1$; and f is the dense phase fraction which determines the weight factors. All parameters and variables in the above model are functions of the operating conditions, bed position, and bed materials.

In order to further characterize the complex two-phase flow structure in timescale, we assumed that the maximum and minimum voidages exist on the ideal center of the bubble phase and the ideal center of the emulsion phase, respectively, and the voidage changes monotonously between the two centers. According to Eqs. (5)–(10), the gas–solid distribution between an emulsion phase element and its neighboring bubble phase element [17] at timescale, called the spatiotemporal gas–solid distribution for convenience, could then be statistically described by a series of local voidages from the ideal center of the emulsion phase element to the ideal center of its neighboring bubble phase element at timescale. The method of equality of probability [19] was used to divide the probability function from ε_{mf} to 1 into n scopes of each probability equal to $1/n$, for which a distance of unit time between the two centers was assumed:

$$\Pr(\varepsilon_{i+1}) - \Pr(\varepsilon_i) = \frac{1}{1-\varepsilon_{mf}} \int_{\varepsilon_i}^{\varepsilon_{i+1}} \mathrm{pr}(\varepsilon)\, \mathrm{d}\varepsilon = \frac{1}{n}, \quad i = 0, 1, \ldots, n-1 \tag{11}$$

where ε_i is the local voidage corresponding to the time coordinate i/n from the center of the emulsion phase element to the center of its neighboring bubble and $\Pr(\varepsilon_i)$ is the cumulative probability of the local voidages from ε_{mf} to ε_i. Eq. (11) gives the dependence of the local voidage (ε_i) with respect to the coordinate (i/n), which can be summarized into a two-dimensional vector $Y = \{(0, \varepsilon_0(\varepsilon_{mf})), (1/n, \varepsilon_1), \ldots, (i/n, \varepsilon_i), \ldots, (1, \varepsilon_n(1))\}$. The spatiotemporal gas–solid distribution shows how gas and solids interpenetrate the bubble and emulsion phases and statistically gives practical flow structure element (from the center of an emulsion phase element to the center of a bubble phase element) at timescale. This can help to understand quantitatively the gas–solid interactions in the fluidized bed.

In order to quantitatively characterize the gas–solid distribution and the influence of the operating conditions thereof, a large number of experiments were conducted using different bed materials. The resulting gas–solid distribution was then developed according to the probability model described above.

3. Experimental

Experiments were carried out in an air-fluidized bed of 152 mm diameter and 1.5 m height under ambient condition and different superficial gas velocities, covering the bubbling and turbulent fluidization regimes. Air was introduced into the bed through a nozzle type distributor placed above a stainless steel porous plate. Two types of particles, namely, FCC (ρ_p=1673 kg/m^3, d_p=70 μm) and irregular sand particles (ρ_p=2650 kg/m^3, d_p=385 μm) with a wide size distribution, as given in Table 1, were used as bed materials to understand and compare the gas–solid distribution of Geldart A and Geldart B particles. The static bed height was 300 mm for all the experiments. The transition superficial gas velocity from bubbling to turbulent fluidization, U_c, was determined by the standard deviation analysis of absolute pressure fluctuations and found to be 0.77 m/s for the FCC particles and 1.50 m/s for the sand particles.

Table 1
Size distribution of the bed materials

Size (μm)	Percentage
FCC	
20	1
40	7
80	50
105	22
149	20
Sand	
90	2.2
180	4.36
250	5.84
417	28.7
595	16.5
850	20.0
1000	30.0

A cross-optical fiber probe with a measurement volume defined by its two cross-fiber bundles of 0.8 mm in diameter, was placed at an axial position of 150 mm above the distributor level and at different radial positions to measure instantaneous voidage. The optical fiber probe was calibrated according to the procedure described by Reh and Li [20]. The measurement volume of the probe employed in this work is very small compared to the size of bubbles. Thus, this probe is sensitive to the local flow pattern and the interaction between bubbles and such probe does not influence the measurements of the actual flow structure.

A PV-4A Particle Velocity Analyzer, made by the Institute of Chemical Metallurgy, Chinese Academy of Sciences, was employed to obtain time series of dynamic voidages. For each run, more than 64 000 data, with a sampling frequency of 488 Hz, were acquired.

4. Results and discussion

4.1. Minimum and maximum voidages

The minimum voidage (ε_{min}) and the maximum voidage (ε_{max}) of the two-phase flow structure were analyzed in order to verify whether or not the emulsion phase and the bubble phase actually show the extreme behavior. In this paper, the voidage corresponding to <1% cumulative probability distribution of the local voidage from ε_{mf} to 1 was

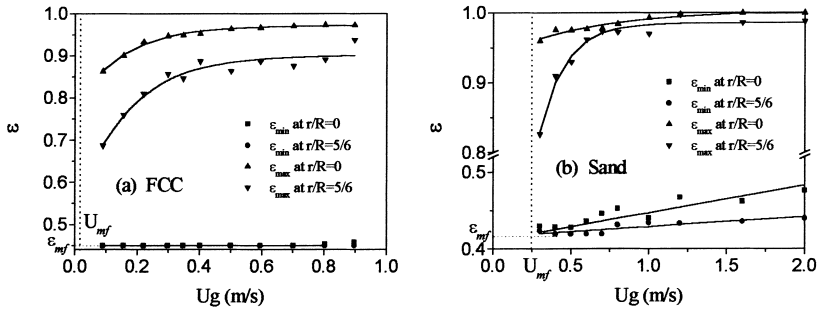

Fig. 2. Change in the minimum voidage of the emulsion phase, ε_{min}, and the maximum voidage of the bubble phase, ε_{max}, with U_g for FCC and sand particles ($r/R=0$ and $r/R=\frac{5}{6}$).

defined as ε_{min}. The voidage corresponding to >99% cumulative probability distribution of the local voidage from ε_{mf} to 1 was defined as ε_{max}. As shown in Fig. 2, the experimental results indicated that for the FCC particles the formation and motion of the bubbles have less effect on the voidage of the emulsion phase and the minimum voidage in the emulsion phase remains almost as that of the saturated emulsion, ε_{mf}, over a wide range of gas velocities. For the sand particles, however, more gas enters and dilutes the emulsion phase and the minimum voidage increases from ε_{mf} almost linearly with increasing U_g, which indicates the increasing degree of dilution of the emulsion phase. On the other hand, the maximum voidage, ε_{max}, exhibits the similar trends for the FCC and sand particles, i.e., rising exponentially with increasing gas velocity at the beginning and then remaining nearly constant at higher gas velocities, as illustrated in Fig. 2. For the sand particles, bubbles seem to be very close to the pure bubbles at higher U_g, while for the FCC particles ε_{max} is considerably lower than unity due to the presence of more particles in the bubbles, as also shown in Fig. 2. Such changes in ε_{min} and ε_{max} with U_g can be expressed as

$$\varepsilon_{min} = \varepsilon_{mf} + k_{min}(U_g - U_{mf}) \quad (12)$$

$$\varepsilon_{max} = k_{max(\infty)} - k_{max(1)} \exp[-(U_g - U_{mf})/k_{max(2)}] \quad (13)$$

where (k_{min}, $k_{max(\infty)}$, $k_{max(1)}$, $k_{max(2)}$)=(0, 0.97, 0.189, 0.115) for the FCC particles, and (k_{min}, $k_{max(\infty)}$, $k_{max(1)}$, $k_{max(2)}$)=(0.034, 1, 0.045, 0.64) for the sand particles, at $r/R=0$. As shown in Fig. 2, the experimental data indicate that the radial position influences the gas–solid distribution. At $r/R=0$, the bubble phase showed the highest ε_{max}, and the emulsion phase was more diluted for the sand particles, while no significant change was observed for the FCC particles.

4.2. Probability distribution function

In order to study the gas–solid distribution of the bubble and emulsion phases, the probability distribution of the local voidage from ε_{mf} to 1 was cumulated according to the method described by Eqs. (5)–(8). It was found that the probability distribution of the local voidage shows nonlinearity, which indicates nonlinear gas–solid distribution in the fluidized beds. The results also show the complex evolution of the probability density function with increasing U_g for both FCC and sand particles. The same phenomena has been observed for MgO particles (d_p=120 μm) [11]. Fig. 3 gives such evolution of the probability distribution for the two types of particles at $r/R=0$. The cumulative probability distribution curves tend to the higher local voidage with increasing U_g as more gas goes into both the emulsion and bubble phases. It is worth mentioning that the probability distribution function changes gradually from bubbling to turbulent fluidization with no abrupt change at U_c.

Fig. 3 also illustrates that the probability distribution of the local voidage for the FCC particles is different from that of the sand particles, even if they both have equal time-averaged voidages. The former has high probability at and nearby the saturation value ε_{mf}, while the latter has very low probability in this region. The emulsion phase strongly shows to be close to the saturated emulsion for the FCC particles, while in the case of the sand particles, the emulsion is far from the saturated state due to the larger amount of the gas entered this phase, as shown in Fig. 3(a) and (b). Therefore, for different fluidized materials, the effect of the gas flow on the emulsion phase is different, their complex two-phase structure behave differently, with different dominant mechanisms for the gas–solid interaction.

The probability distribution of the local voidage and its evolution also depends on the radial position for both particles, as shown in Fig. 4. The evolution of the probability distribution function occurs to a greater extent on the bed core compared to that near the wall for the same gas velocity. Most runs show the highest cumulative probability near the wall and the lowest at $r/R=0$, since more gas flows through the center of the bed than close to the wall. The gas–solid distribution greatly depends on the gas velocity, the bed position and the particle properties, which indicates the complexity of quantifying the dynamic behavior of the gas and solids in fluidized bed.

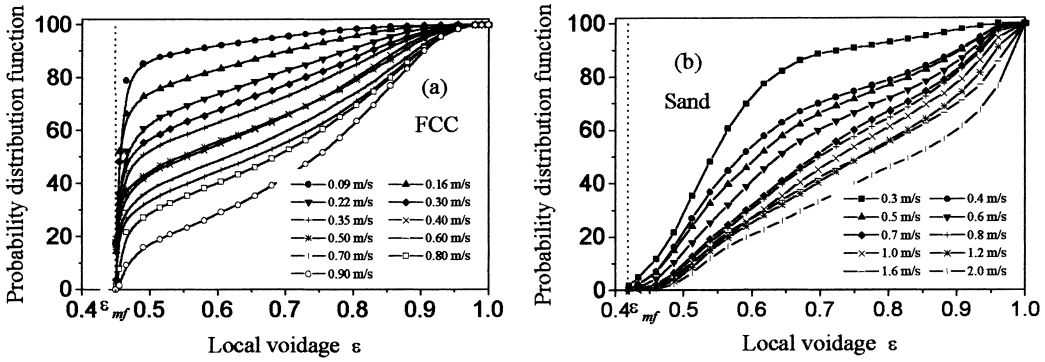

Fig. 3. Evolution of the probability distribution function of the local voidage with U_g at r/R=0: (a) FCC; (b) sand.

4.3. Probability density function

The probability density function of the local voidage, pr(ε), as expressed in Eqs. (5)–(10), was further analyzed to quantitatively explain the gas–solid distribution and its dependence on both the operating conditions and particle properties. This is allowed for exploring the dynamic behavior of the bubble and emulsion phases. It was found that the local voidage from ε_{mf} to 1 exhibits a double-peak probability density function for both particles tested, one peak for the emulsion phase and another peak for the bubble phase. The double-peak probability density curve changes upon increasing gas velocity, U_g. An increase in the gas velocity results in decreasing the probability density of the emulsion phase and increasing the probability density of the bubble phase. The average peak voidage of the emulsion phase is found to be equal or close to ε_{mf} for FCC particle and $\varepsilon \approx 0.55$ ($>\varepsilon_{mf}$) for the sand particles and the average peak voidage of the bubble phase was found to be $\varepsilon \approx 0.85$ for FCC particles and $\varepsilon \approx 0.95$ for the sand particles at r/R=0, as shown in Fig. 5(a) and (b).

Such a probability density function and its evolution also depends on the radial position for both particles tested, as shown in Fig. 6(a1) and (a2) (r/R=0 and $\frac{5}{6}$). The peak for the emulsion decreases gradually and the peak for the bubbles increases gradually from the wall to the core at the same gas velocity. Furthermore, the same observation still applies with the same time-averaged voidage in different positions as shown in Fig. 6(b1) and (b2). In this case, the probability

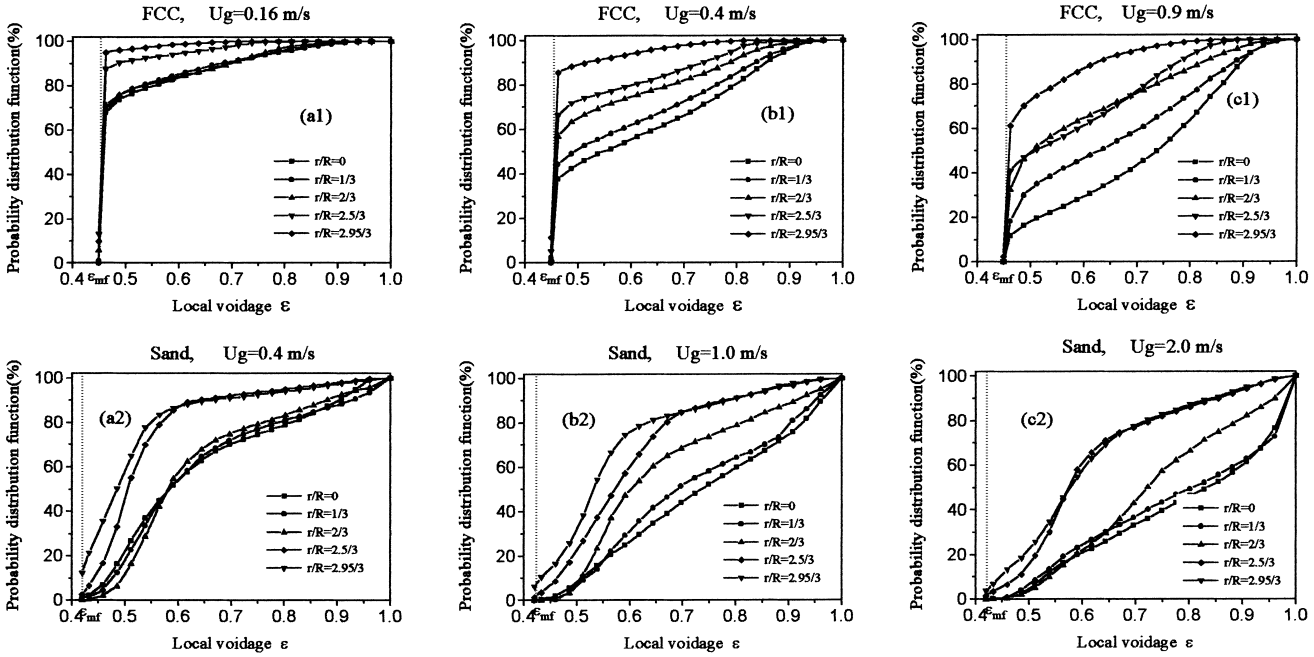

Fig. 4. Comparison between the probability distribution functions of the local voidage at different radial positions and different U_g: (a1), (b1), (c1) FCC; (a2), (b2), (c2) sand.

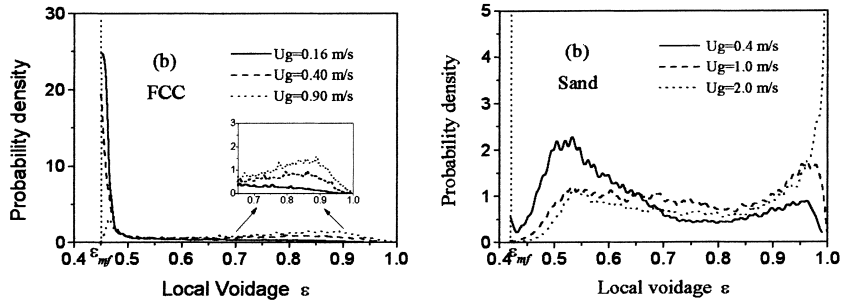

Fig. 5. Change in the probability density function of the local voidage with U_g at r/R=0: (a) FCC; (b) sand.

density for the bubbles is lower near the wall than in the core. As suggested by the data in Fig. 6, the wall has a strong effect on the gas–solid distribution in the emulsion and bubble phases.

4.4. Quantification of the probability density function

Although the gas–solid distribution showed the double-peak probability density function, the density function corresponding to the two phases are continuous for both the particles tested. In order to describe such a gas–solid distribution with the two-peak density function, the minimum probability method was introduced to determine the division (ε_{div}) between the emulsion phase and the bubble phase, i.e., to take the local voidage point with the minimum probability density between the two peaks as the division. The division, ε_{div}, was found to change with gas velocity and the bed position in both bubbling and turbulent regimes, which could be correlated as

$$\varepsilon_{div} = k_{div\,0} + k_{div\,1}(U_g - U_{mf}) \quad (14)$$

where ($k_{div\,0}$, $k_{div\,1}$)=(0.548, 0.027) for the FCC particles and ($k_{div\,0}$, $k_{div\,1}$)=(0.815, 0.029) for the sand particles at r/R=0. The division between two phases is different for different particles.

By using such a division, ε_{div}, for both FCC and sand particles the probability density function of the local voidage of the emulsion phase and that of the bubble phase could be found to satisfy the beta distribution under various operating conditions. The complex double-peak probability density of the local voidage from ε_{mf} to 1 and its change could be quantified by the density function of a particular distribution, called the coupled beta distribution. This density function can be obtained by coupling two beta probability density

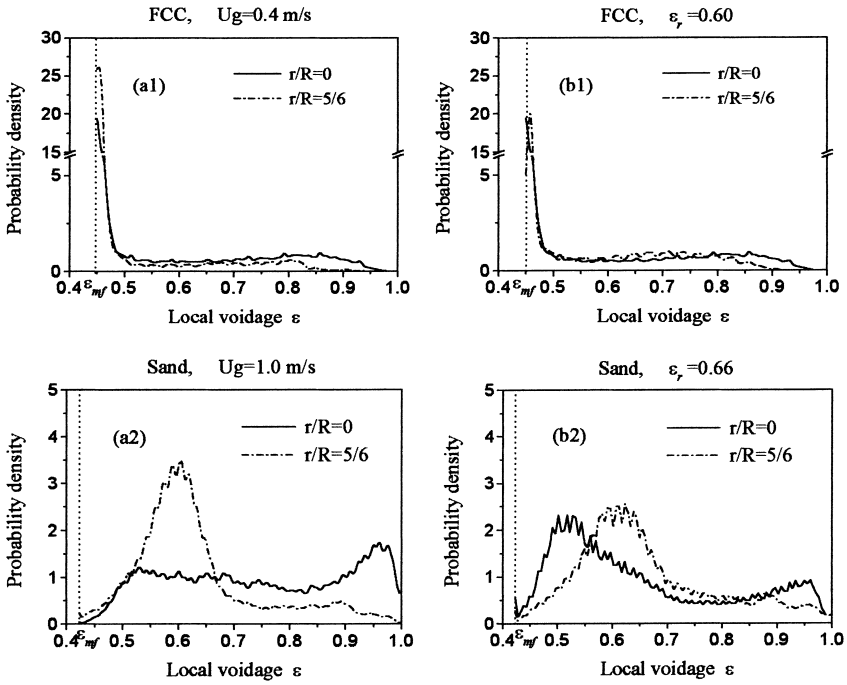

Fig. 6. Comparison between the probability density functions of the local voidage at different radial positions: (a1), (b1) FCC; (a2), (b2) sand; (a1), (a2) for the same U_g; (b1), (b2) for the same time-averaged voidage.

functions, one for the emulsion phase and another for the bubble phase, i.e., in Eq. (10), taking

$$\mathrm{pr_b}(\varepsilon) = \frac{\varepsilon^{\alpha_b-1}(1-\varepsilon)^{\beta_b-1}}{B(\alpha_b, \beta_b)} \times (\text{beta probability density function}) \quad (15)$$

$$\mathrm{pr_e}(\varepsilon) = \frac{\varepsilon^{\alpha_e-1}(1-\varepsilon)^{\beta_e-1}}{B(\alpha_e, \beta_e)} \times (\text{beta probability density function}) \quad (16)$$

Thus

$$\mathrm{pr}(\varepsilon) = f\frac{\varepsilon^{\alpha_e-1}(1-\varepsilon)^{\beta_e-1}}{B(\alpha_e, \beta_e)} + (1-f) \times \frac{\varepsilon^{\alpha_b-1}(1-\varepsilon)^{\beta_b-1}}{B(\alpha_b, \beta_b)}, \quad \varepsilon_{mf} \le \varepsilon \le 1 \times (\text{coupled beta probability density function}) \quad (17)$$

where

$$B(\alpha_k, \beta_k) = \frac{\Gamma(\alpha_k)\Gamma(\beta_k)}{\Gamma(\alpha_k+\beta_k)}, \quad (k = \mathrm{e, b}) \quad (\text{beta function}) \quad (18)$$

$$\Gamma(t) = \int_0^\infty x^{t-1}\mathrm{e}^{-x}\,\mathrm{d}x, \quad t > 0 \quad (\text{gamma function}) \quad (19)$$

$$f = \frac{\varepsilon_b - \varepsilon_r}{\varepsilon_b - \varepsilon_e} \quad (\text{emulsion phase fraction}) \quad (20)$$

$$\alpha_e = \varepsilon_e\left[\frac{\varepsilon_e(1-\varepsilon_e)}{{\sigma_e}^2} - 1\right] \quad (21)$$

$$\beta_e = (1-\varepsilon_e)\left[\frac{\varepsilon_e(1-\varepsilon_e)}{{\sigma_e}^2} - 1\right] \quad (22)$$

$$\alpha_b = \varepsilon_b\left[\frac{\varepsilon_b(1-\varepsilon_b)}{{\sigma_b}^2} - 1\right] \quad (23)$$

$$\beta_b = (1-\varepsilon_b)\left[\frac{\varepsilon_b(1-\varepsilon_b)}{{\sigma_b}^2} - 1\right] \quad (24)$$

where ε_e and σ_e are the mean and variance of the beta distribution for the voidage fluctuations in the emulsion phase and ε_b and σ_b are the mean and variance of the beta distribution of the voidage fluctuations in the bubble phase, estimates of which may be given as

$$\varepsilon_e = \frac{1}{m_1}\sum_{i=1}^{m_1}\varepsilon_{e(i)}, \qquad \hat{\varepsilon}_b = \frac{1}{m_2}\sum_{j=1}^{m_2}\varepsilon_{b(j)} \quad (25)$$

$$\sigma_e = \sqrt{\frac{1}{m_1-1}\sum_{i=1}^{m_1}(\varepsilon_{e(i)} - \varepsilon_e)^2}, \qquad \sigma_b = \sqrt{\frac{1}{m_2-1}\sum_{j=1}^{m_2}(\varepsilon_{b(j)} - \varepsilon_b)^2} \quad (26)$$

Figs. 7 and 8 show part of the experimental results achieved with two different particles. The voidage fluctuations, both in the emulsion phase and in the bubble phase, change with operating conditions. By increasing U_g in a moderate range, gradual increase is observed in the bubble phase fraction ($1-f$), the time-averaged voidage ε_r, the mean voidage of each phase (ε_e, ε_b), the mean variance σ, the variance for emulsion phase σ_e, and the variance for bubble phase σ_b, due to the stronger action of the gas. At higher gas velocities, though, these variables remain constant in the bed core, as shown in Fig. 7. It can be seen from Figs. 7 and 8 that the two types of the particles provide different voidage fluctuations in the two phases. All these phenomena can be correlated with the operating conditions as follows:

$$f = A_{f(1)} + A_{f(2)}\exp[-(U_g - U_{mf})/A_{f(3)}] \quad (27)$$

$$\varepsilon_b = A_{\text{void-b}(1)} + A_{\text{void-b}(2)}\exp[-(U_g - U_{mf})/A_{\text{void-b}(3)}] \quad (28)$$

$$\varepsilon_e = A_{\text{void-e}(1)} + A_{\text{void-e}(2)}\exp[-(U_g - U_{mf})/A_{\text{void-e}(3)}] \quad (29)$$

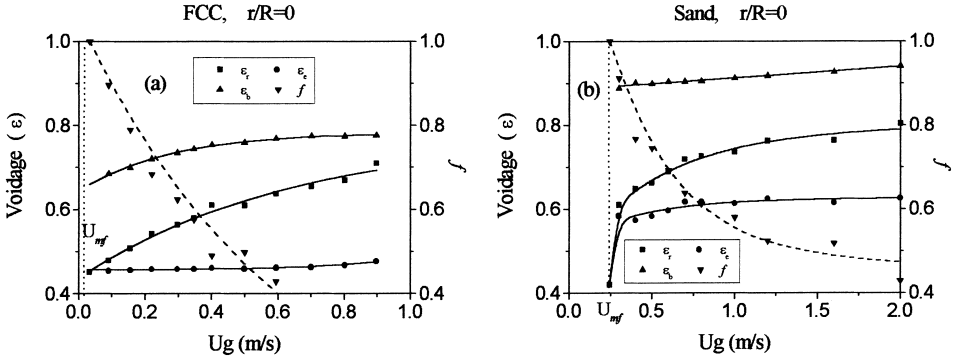

Fig. 7. Change in the emulsion phase fraction, the time-averaged voidage, and the mean voidages of the bubble phase and the emulsion phase with U_g at r/R=0: (a) FCC; (b) sand.

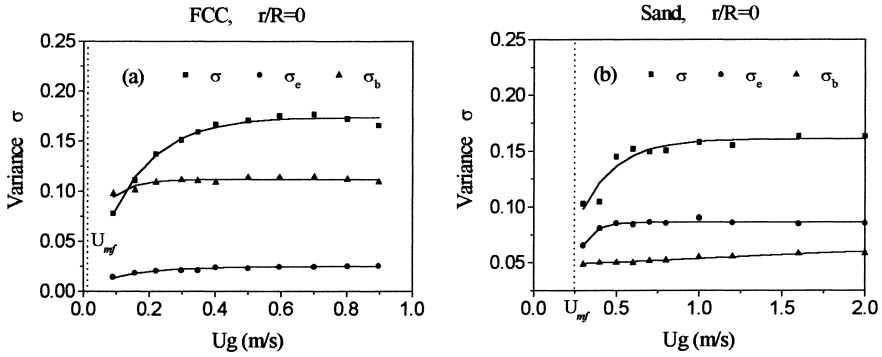

Fig. 8. Change in the mean variance of voidage fluctuations, and the variances of voidage fluctuations in the emulsion phase and the bubble phase with U_g at r/R=0: (a) FCC; (b) sand.

Table 2
The values of parameters in Eqs. (27)–(31) (r/R=0)

	FCC	Sand
$A_{f(1)}$	0	0.466
$A_{f(2)}$	1.00	0.534
$A_{f(3)}$	0.62	0.413
$A_{\text{void-b(1)}}$	0.784	1.0
$A_{\text{void-b(2)}}$	−0.139	−0.146
$A_{\text{void-b(3)}}$	0.272	4.439
$A_{\text{var-b(1)}}$	0.112	0.065
$A_{\text{var-b(2)}}$	−0.116	−0.017
$A_{\text{var-b(3)}}$	0.047	1.57
$A_{\text{void-e(1)}}$	ε_{mf}	ε_{mf}+0.20
$A_{\text{void-e(2)}}$	0.00061	−0.059
$A_{\text{void-e(3)}}$	−0.262	0.429
$A_{\text{var-e(1)}}$	0.025	0.086
$A_{\text{var-e(2)}}$	−0.02	−0.0408
$A_{\text{var-e(3)}}$	0.152	0.074

$$\sigma_{\text{b}}=A_{\text{var-b(1)}}+A_{\text{var-b(2)}}\exp[-(U_{\text{g}}-U_{\text{mf}})/A_{\text{var-b(3)}}] \quad (30)$$

$$\sigma_{\text{e}}=A_{\text{var-e(1)}}+A_{\text{var-e(2)}}\exp[-(U_{\text{g}}-U_{\text{mf}})/A_{\text{var-e(3)}}] \quad (31)$$

Table 2 gives the values of the parameters in the above correlation at r/R=0. The relation between the dense phase fraction and the saturated emulsion phase fraction from simple two-phase model, described by Eq. (4), was found as

$$f=(A_{f0(1)}+A_{f0(2)}(U_{\text{g}}-U_{\text{mf}}))f^0 \quad (32)$$

where at r/R=0, for the FCC particles ($A_{f0(1)}$, $A_{f0(2)}$)= (0.95, 1.17), and for the sand particles ($A_{f0(1)}$, $A_{f0(2)}$)= (1.29, 0). Since $A_{f0(2)}$=0 for sand, the dense phase fraction is proportional to the assumed saturated emulsion fraction.

By using estimated values of f, α_{e}, β_{e}, α_{b}, and β_{b} obtained from Eqs. (20)–(24) and the corresponding correlations of the mean voidage and the variance in the two phases, the probability density of the local voidage was simulated with the density function described by Eq. (17). Fig. 9 gives the comparison between the simulated results with the corresponding experimental data. The chi-square (χ^2) statistical test [21] shows a good agreement between the simulated and the experimental data. Therefore, the probability density of the local voidage from ε_{mf} to 1 for both the FCC and sand particles and its changes with operating conditions can be described and simulated effectively by the density function of the so-called coupled beta distribution.

4.5. Transition from bubbling to turbulent regime

Fig. 10 shows the simulated evolution of the probability density function of the local voidage at r/R=0, as described by Eq. (17). It can be seen from Fig. 10 that the probability density of the bubble phase becomes higher and that of the

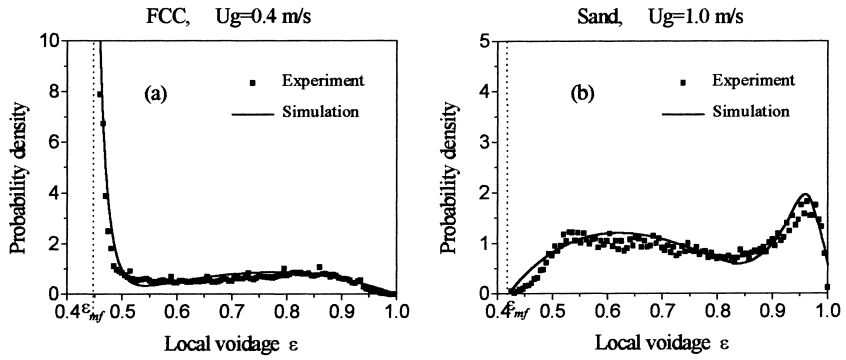

Fig. 9. Comparison between experimental and simulated probability density functions of the local voidage (r/R=0).

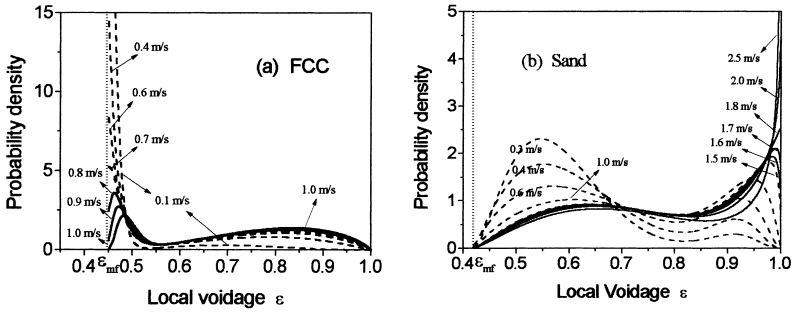

Fig. 10. Simulated probability density function of the local voidage and its change with gas velocity (r/R=0; dash line: bubbling regime, solid line: turbulent regime).

dense phase becomes lower with increasing U_g. It can also be concluded from this figure that the gas-solid distribution evolves gradually from bubbling to turbulent regime. Nevertheless, two different states of gas-solid distribution can be observed in these regimes and this difference is distinct for each particle type.

In the case of FCC particles (Fig. 10(a)), the fraction of the emulsion phase reduces upon increasing the gas velocity. However, in the bubbling regime the maximum density appears at ε_{mf}, while in the turbulent regime an apparent change in the shape of the probability density function can be observed and the maximum density gradually departs from ε_{mf} and the saturated emulsion tends to disappear due to more intensive action of gas. Moreover, the probability density of the bubble phase in fluidized FCC particles does not exhibit considerable difference in the turbulent regime which suggests that beyond U_c the excess gas enters and dilutes the emulsion rather than forming more bubbles and increasing the bubble phase fraction.

In the case of sand particles (Fig. 10(b)), increasing the superficial gas velocity results in decreasing the solid content of the bubbles and the bubble phase becomes more dilute. This, of course, means larger gas core in bubbles of a bed of sand particles. Upon approaching U_c, the bubble phase displays noticeable change in its probability density. With increasing the gas velocity beyond U_c, the probability density of the pure bubble (ε=1) gradually rises and the voidage of the maximum probability density of the bubble phase approaches unity. Furthermore, the probability density of the emulsion phase does not show significant difference in the turbulent regime, which suggests that at superficial gas velocities higher than U_c, the excess gas enters the bubble phase and increases the bubble phase fraction rather than entering and diluting the emulsion.

The change in the state of the emulsion and bubble phases is more explicitly shown in Fig. 11(a) and (b) for FCC and sand particles, respectively. Fig. 11(a) demonstrates the change in the probability of the local voidage $\varepsilon=\varepsilon_{mf}$ for FCC particles and shows that the probability of the emulsion being at its saturation state ($\varepsilon=\varepsilon_{mf}$) is very high at low gas velocities and constantly decreases upon increasing the gas velocity. At superficial gas velocities near U_c, this probability is very close to zero, which indicates that the saturation emulsion almost diminishes at the transition from bubbling to turbulent. Fig. 11(b) shows the change in the probability of the local voidage ε=1 for sand particles and indicates that pure bubble (ε=1) does not exist at low gas velocities. However, at superficial gas velocity near U_c, the pure bubble begins to occur and its probability increases upon increasing the gas velocity.

4.6. Spatiotemporal gas–solid distribution

According to Eqs. (11) and (17), the spatiotemporal gas–solid distribution between the two phases was statistically described and simulated by the dependence of the local voidage on the coordinate from the ideal center of the emulsion phase element to the ideal center of its

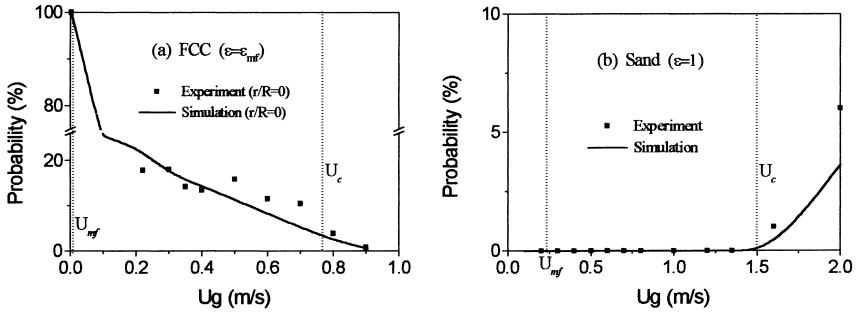

Fig. 11. Changes in the probability of the local voidage $\varepsilon=\varepsilon_{mf}$ for the FCC particles and of the local voidage ε=1 for the sand particles.

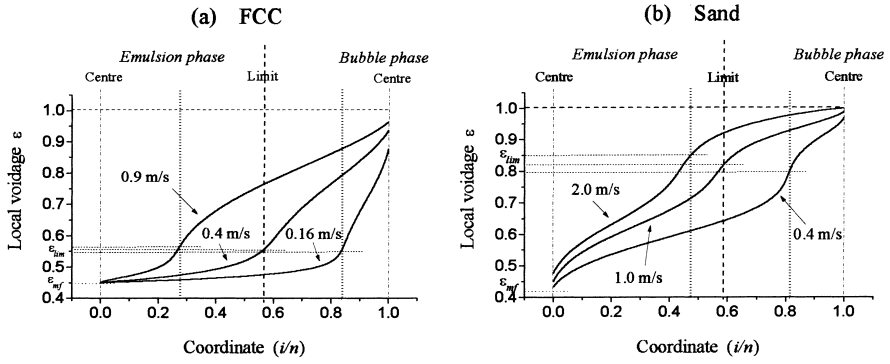

Fig. 12. Spatiotemporal voidage distribution between two centers of an emulsion phase element and its neighboring bubble phase at timescale (r/R=0).

neighboring bubble, i.e., in the vector $Y = \{(0, \varepsilon_{\min}), (1/n, \varepsilon_1), \ldots, (i/n, \varepsilon_i), \ldots, (1, \varepsilon_{\max})\}$, ($\varepsilon_{\mathrm{mf}}$, 1) should be replaced with ($\varepsilon_{\min}$, $\varepsilon_{\max}$). Fig. 12 shows the dependence of the local voidage ε_i on the time coordinates i/n and the influence of the gas velocity at r/R=0 for the FCC and sand particles. It also indicates a considerable difference in the gas–solid distribution and two-phase flow structures (the bubble structure and the emulsion structure), suggesting different dominant mechanisms influencing the gas–solid interactions for different particles. Such analysis also gives an experimental support to the model proposed by Gilbertson and Yates [9], i.e., inertia allows some particles to penetrate into bubbles and the extent of the penetration is influenced by the particle properties. Different particles result in different bubble structures.

The above description of the probability distribution of the local voidage and the spatiotemporal gas–solid distribution can contribute to further quantitative characterization of the gas–solid interaction, mass transfer and reaction rates in fluidized beds.

5. Conclusion

A probability distribution model of the local voidage was developed to describe and simulate the gas–solid distribution in the fluidized bed reactors. The two different particles tested (FCC and sand) exhibited considerably different dynamic gas–solid distributions and two-phase flow structures, implying different dominant mechanisms ruling their gas–solid interactions. For FCC particles, the voidage of the emulsion phase with the highest probability is close to $\varepsilon_{\mathrm{mf}}$ in bubbling regime, increasing gradually in the turbulent regime due to more intensive action of gas. However, for the sand particles this voidage of the emulsion phase differs greatly from $\varepsilon_{\mathrm{mf}}$. The bubble phase becomes more dilute at higher U_{g}, and the probability of the pure bubble increase gradually in turbulent regime. It is worth mentioning that this conclusion does not mean that less solid particles enter the bubbles at higher superficial gas velocities, but indicates that the pure gas region in the center of the bubble grows larger with increasing gas velocity. In this case, the gas enters the bubble at a rate higher than the particles, resulting in an overall more dilute bubble phase at higher gas velocities.

The probability distribution function showed gradual evolution with superficial gas velocity, suggesting that there is no abrupt change in the two-phase flow structure in transition from bubbling to turbulent fluidization. However, in the case of FCC particles, the gas mostly enters and dilutes the emulsion phase constantly at velocities higher than U_{c}. For the sand particles, increasing the gas velocity beyond U_{c} results in forming more pure bubbles. The probability distribution function also showed a strong dependency on the radial position and particle type. By using the minimum probability method to identify the division between the emulsion and bubble phases, the voidage fluctuations of the two phases were found to follow beta distribution, and the probability density function of the local voidage from $\varepsilon_{\mathrm{mf}}$ to 1 and its complex evolution from bubbling to turbulent fluidization regime could be effectively described and simulated by the coupled beta distribution. Such quantification further introduced statistically the spatiotemporal gas–solid distribution of the two-phase flow structure at timescale.

6. Nomenclature

$A_{f(i)}$	parameter of Eq. (27), i=1, 2, 3
$A_{f0(i)}$	parameter of Eq. (32), i=1, 2
$A_{\text{var-b}(i)}$	parameter of Eq. (30), i=1, 2, 3
$A_{\text{var-e}(i)}$	parameter of Eq. (31), i=1, 2, 3
$A_{\text{void-b}(i)}$	parameter of Eq. (28), i=1, 2, 3
$A_{\text{void-e}(i)}$	parameter of Eq. (29), i=1, 2, 3
d_{p}	average particle diameter (μm)
f	dense phase (emulsion phase) fraction
f^0	emulsion phase fraction in simple two-phase model
$k_{\mathrm{div}\,0}$	parameter of Eq. (14)
$k_{\mathrm{div}\,1}$	parameter of Eq. (14)
$k_{\max(1)}$	parameter of Eq. (13)
$k_{\max(2)}$	parameter of Eq. (13)
$k_{\max(\infty)}$	parameter of Eq. (13)

k_{min}	parameter of Eq. (12)
m_1	number of samples for emulsion phase
m_2	number of samples for bubble phase
n	number of scopes of equality probability in total
$Pr^0(\varepsilon)$	probability distribution function of local voidages for the two extreme phases
$Pr_b{}^0(\varepsilon)$	probability distribution function of local voidages for pure bubble phase
$Pr_e{}^0(\varepsilon)$	probability distribution function of local voidages for saturated emulsion phase
$Pr(\varepsilon)$	probability distribution function of local voidages for the two phases
$Pr_b(\varepsilon)$	probability distribution function of local voidages for dynamic bubble phase
$Pr_e(\varepsilon)$	probability distribution function of local voidages for dynamic emulsion phase
$pr(\varepsilon)$	probability density function of local voidages for the two phases
$pr_b(\varepsilon)$	probability density function of local voidages for dynamic bubble phase
$pr_e(\varepsilon)$	probability density function of local voidages for dynamic emulsion phase
r/R	dimensionless radius of bed
U_c	transition superficial gas velocity from bubbling to turbulent fluidization (m/s)
U_g	superficial gas velocity (m/s)
U_{mf}	minimum fluidization gas velocity (m/s, 0.003 m/s for FCC; 0.24 m/s for sand)
Y	vector of voidages and positions

Greek symbols

α_i	parameter in beta distribution, i=e, b
β_i	parameter in beta distribution, i=e, b
ε	local voidage from ε_{mf} to 1
ε_b	mean voidage of bubble phase
ε_{div}	division of local voidage between bubble phase and emulsion phase
ε_e	mean voidage of emulsion phase
ε_i	local voidage corresponding to time coordinate i/n between two centers
ε_{max}	maximum local voidage
ε_{mf}	minimum fluidization voidage (0.45 for FCC; 0.42 for sand)
ε_{min}	minimum local voidage
ε_r	time-averaged voidage at an arbitrary radial position
ρ_p	particle density (kg/m^3)
σ_b	variance of voidage fluctuations in bubble phase
σ_e	variance of voidage fluctuations in emulsion phase

Subscripts

b	bubble phase
e	emulsion phase

Acknowledgements

The authors gratefully acknowledge the financial support from the Natural Sciences and Engineering Research Council of Canada (NSERC), and also wish to thank Mr. Pierre Sauriol for his effort in improving the manuscript.

References

[1] J.F. Davidson, et al. (Eds.), Fluidization, 2nd Edition, Academic Press, London, 1985.
[2] J.E. Johnson, J.R. Grace, J.J. Graham, Fluidized-bed reactor model verification on a reactor of industrial scale, AIChE J. 33 (1986) 619–627.
[3] M. Pell, Gas Fluidization, Elsevier, Amsterdam, 1990.
[4] D. Kunii, O. Levenspiel, Fluidization Engineering, 2nd Edition, Butterworth-Heinemann, Boston, MA, 1991.
[5] R. Toei, R. Matsuno, The coalescence of bubbles in the gas–solid fluidized bed, in: A.A.H. Drinkenburg (Ed.), Proceedings of the International Symposium on Fluidization, Netherlands University Press, Amsterdam, 1967.
[6] M. Aoyagi, D. Kunii, Importance of dispersed solids in bubbles for exothermic reactions in fluidized beds, Chem. Eng. Commun. 1 (1974) 191–197.
[7] J.R. Grace, Generalized models for isothermal fluidized bed reactors, Recent Advances in Engineering Analysis of Chemically Reacting System, Wiley, New York, 1984, pp. 237–255.
[8] G.K. Batchelor, J.M. Nitsche, Expulsion of particles from a buoyant blob in a fluidized bed, J. Fluid Mech. 278 (1994) 63–81.
[9] M.A. Gilbertson, J.G. Yates, The motion of particles near a bubble in a gas-fluidized bed, J. Fluid Mech. 323 (1996) 377–385.
[10] A.R. Abrahamson, D. Geldart, Behaviour of gas-fluidized beds of fine powders. Part II. Voidage of the dense phase in bubbling beds, Powder Technol. 26 (1980) 47–55.
[11] J. Chaouki, A. Gonzalez, C. Guy, D. Klvana, Two-phase model for a catalytic turbulent fluidized-bed reactor: application to ethylene synthesis, Chem. Eng. Sci. 54 (1999) 2039–2045.
[12] Yu.A. Buyevich, Sh.K. Kapbasov, Random fluctuations in fluidized beds, Chem. Eng. Sci. 49 (1994) 1229–1243.
[13] J.H. Li, L.X. Wen, W. Ge, H.P. Cui, J.Q. Ren, Dissipative structure in concurrent-up gas–solid flow, Chem. Eng. Sci. 53 (1998) 3367–3379.
[14] A. Marzocchella, R.C. Zijerveld, J.C. Schouten, C.M. van den Bleek, Chaotic behavior of gas–solids flow in the riser of a laboratory-scale circulating fluidized bed, AIChE J. 43 (1997) 1458–1468.
[15] D. Musmarra, M. Poletto, S. Vaccaro, R. Clift, Dynamic waves in fluidized beds, Powder Technol. 82 (1995) 255–268.
[16] D. Bai, A.S. Issangya, J.R. Grace, Characteristics of gas-fluidized beds in different flow regimes, Ind. Eng. Chem. Res. 38 (1999) 803–811.
[17] H.P. Cui, J.H. Li, M. Kwauk, H.Zh. An, M. Chen, Zh.M. Ma, G.F. Wu, Dynamic behaviors of heterogeneous flow structure in gas–solid fluidization (special issue), Powder Technol. 112 (2000), in press.
[18] J.H. Li, L.X. Wen, G.H. Qian, H.P. Cui, M. Kwauk, J.C. Schouten, C.M. van den Bleek, Structure heterogeneity, regime multiplicity and nonlinear behavior in particle–fluid systems, Chem. Eng. Sci. 51 (1996) 2693–2698.
[19] Z.L. Lehmann, Testing Statistical Hypothesis, 2nd Edition, Wiley, New York, 1986.
[20] L. Reh, J. Li, Measurement of voidage in fluidized beds by optical probes, in: P. Basu, M. Horio, M. Hasatani (Eds.), Circulating Fluidized Bed Technology III, Pergamon, Oxford, 1991, pp. 163–170.
[21] R.V. Hogg, E.A. Tanis, Probability and Statistical Inference, 3rd Edition, Macmillan, New York, 1977.